Key Engineering Materials
ISSN: 1662-9795, Vol. 1048, pp 151-164
doi:10.4028/p-3rVfXq

Submitted: 2026-01-19
Revised: 2026-02-16
Accepted: 2026-02-25
Online: 2026-04-14

Transient Thermal Analysis of Multiple Extrusion Runs with Nitrogen Cooling by Means of Qform Code

Riccardo Pelaccia[1,a*], Sara Di Donato[2,b], Marco Negozio[3,c], Nicola Lai[2,d], Barbara Reggiani[1,4 e] and Lorenzo Donati[2,f]

[1]DISMI – University of Modena and Reggio Emilia, via Amendola 2, 42122, Reggio Emilia, Italy

[2]DIN- University of Bologna , Viale Risorgimento 2, 40136, Bologna, Italy

[3]DISTI- University of Parma, Parco Area delle Scienze, 181/A, 43124 Parma, Italy

[4]INTERMECH – University of Modena and Reggio Emilia, Piazzale Europa 1, 42124, Reggio Emilia, Italy

[a]riccardo.pelaccia@unimore.it, [b]sara.didonato2@unibo.it, [c]marco.negozio@unipr.it, [d]nicola.lai5@unibo.it [e]barbara.reggiani@unimore.it, [f]l.donati@unibo.it

Keywords: Nitrogen Cooling, Extrusion, Advanced Numerical Simulation, AA6082

Abstract. In hot extrusion of light alloys, nitrogen cooling has become a strategic solution to mitigate thermal issues from high deformation rates and frictional heating, improving surface quality, extrusion speed, and die life. However, current cooling system designs remain largely empirical, and the limited use of predictive modeling and experimental monitoring often leads to inconsistent evaluations. This work proposes a dual-step procedure for transient numerical analysis of multiple billets with nitrogen cooling. First, a 1D numerical model of nitrogen cooling is simulated in a simplified environment reproducing extrusion thermal conditions, requiring negligible computational time. The resulting heat transfer coefficient (HTC) and nitrogen temperature are then integrated into the process model, implemented in Qform code, as additional boundary conditions. This approach enables the fully 3D extrusion model to account for nitrogen cooling effects not only on thermal gradients but also on aluminium flow and die resistance. A porthole die with three tube-shaped openings for hollow profile extrusion was experimentally tested under cooled and uncooled conditions, with thermal behaviour monitored by eleven thermocouples within the tooling set. Experimental–numerical comparison confirmed the advantages of numerical simulation for cooling channel design and the limitations of experience-based approaches.

1 Introduction

The aluminum extrusion process is widely employed for the production of lightweight structural components with complex cross-sections; however, its efficiency and product quality are strongly constrained by the severe thermal loads acting on the extrusion die during operation [1-2]. Frictional heating at the billet–tool interfaces and plastic deformation lead to localized temperature peaks, particularly in the bearing zones, which can result in uneven material flow, surface defects, accelerated die wear, and limitations on achievable extrusion speed [1-2]. Experimental benchmark studies on industrial extrusion processes have clearly demonstrated that temperature control within the die is a key factor governing profile dimensional accuracy, microstructural homogeneity, and tool deflection [3-6]. In this context, nitrogen cooling has progressively emerged as a promising solution for advanced thermal management in hot extrusion processes, owing to the favorable thermophysical properties of nitrogen and its inert chemical nature.

Experimental investigations conducted over the last decades have demonstrated that both gaseous and liquid nitrogen can be effectively employed to control die temperature, stabilize process conditions, and improve extrudate quality. Industrial trials based on gaseous nitrogen cooling integrated into extrusion dies have shown measurable reductions in exit temperature and significant improvements in production efficiency, enabling higher ram speeds while maintaining acceptable surface quality and process stability [7-8]. More pronounced effects have been reported for liquid nitrogen cooling, which, due to the combination of low boiling temperature (-196°C at 1 bar pressure)

and good latent heat (of the order of 200 kJ/kg), enables intense localized heat extraction in critical die regions. Experimental campaigns on AA6xxx alloys have demonstrated that liquid nitrogen cooling of the tooling set can reduce bearing-zone temperatures by several tens of degrees Celsius [9], improve surface finish and reduce oxidation [10], without inducing a significant increase in extrusion force [9]. Recent studies have further confirmed that liquid nitrogen cooling allows stabilization of exit temperature even at increased ram speeds, thus extending the feasible process window and improving productivity [11-12].

Despite these clear experimental advantages, the industrial implementation of nitrogen cooling systems remains largely based on empirical design practices [13]. In conventional extrusion tooling, cooling channels are typically manufactured by drilling and milling operations in the backer, which severely limits their geometric complexity and their proximity to the most thermally critical regions of the die, particularly the bearing zones. Consequently, cooling effectiveness strongly depends on experience-based decisions regarding channel layout, cross-section, and nitrogen flow conditions. The use of liquid nitrogen introduces additional challenges associated with premature phase change inside the channels, where the rapid liquid-to-gas transition causes drastic volumetric expansion, flow instabilities, and local obstruction of the cooling path, ultimately resulting in non-uniform cooling and inefficient nitrogen consumption [5,6,9,13]. In addition, cooling performance is still assessed indirectly through surface appearance of the extruded profile rather than through direct evaluation of the thermal field within the die, which may lead to misleading conclusions and suboptimal use of nitrogen cooling technology.

In parallel, advances in additive manufacturing and rapid tooling technologies, such as selective laser melting, have enabled the fabrication of conformal cooling channels that closely follow die geometry and target thermal hot spots more effectively than conventional straight-drilled channels [14-15]. Although most applications of conformal cooling have been reported for die casting and injection molding [16-17], some studies highlight their strong potential for extrusion dies, even if industrial adoption of additive technology is still limited [14-15,18].

In this context, to support the design and optimization of nitrogen cooling systems in extrusion dies, some numerical modeling approaches have been proposed in recent literature. Simplified, but very fast, approaches based on constant heat transfer coefficients are unable to capture the thermo-fluid-dynamic behavior of nitrogen flow and the effects of phase change [19]. More advanced three-dimensional coupled fluid–thermal models can represent nitrogen flow and heat transfer in detail, but their computational cost makes them impractical for iterative design and industrial deployment. As a compromise, one-dimensional models of cooling channels have been developed, in which the cooling path is reduced to its midline and key parameters such as pressure drop, Reynolds number, Nusselt number, and heat exchange are evaluated as functions of geometry and operating conditions. These models have been successfully coupled with three-dimensional finite element simulations of the extrusion process, allowing realistic analysis of the thermal field without excessive computational effort [13,15,19]. A significant advancement in this framework is the application of the homogeneous flow model (HFM), which treats the liquid–gas nitrogen mixture as a single equivalent fluid with pseudo-properties evolving with temperature and vapor quality [20]. By implicitly accounting for phase change effects without explicitly resolving evaporation phenomena, the HFM provides a robust balance between predictive accuracy and numerical efficiency, with validation studies under industrial extrusion conditions showing temperature prediction errors typically below 10% [19, 21].

Building upon these modeling approaches, recent numerical studies have integrated the simulation of the process with optimization algorithms to improve channel design. Size optimization and path optimization strategies have been applied to reduce thermal non-uniformity in the bearing zones while simultaneously minimizing nitrogen consumption, demonstrating that even moderate modifications of channel geometry can lead to substantial improvements in cooling performance and die life [19,22].

At the same time, commercial finite element software packages dedicated to aluminum extrusion, such as QForm and HyperXtrude, have reached a high level of maturity in the simulation of material flow, temperature evolution, die stresses, defect formation, and microstructure evolution, and are

widely used for industrial die design and process optimization. For example, Biba et al. [23-24] employed QForm-Extrusion to perform a fully coupled simulation of material flow and die deformation in complex-shape extrusion, showing that die elastic deflection significantly affects velocity distribution and final profile geometry, thereby highlighting the importance of die–process interaction in extrusion design. Koloskov et al. [25] demonstrating Qform capability to accurately simulate semi-continuous extrusion of hollow AA6063 profiles, capturing metal flow distribution and temperature evolution along the die and calibrator with good agreement to industrial observations. Similarly, Hoque et al. [26] used HyperXtrude to compare different friction models in hot forward extrusion of EN AW-6060 and EN AW-6082 alloys, demonstrating that friction law selection has a strong impact on predicted strain, temperature, and extrusion force, with direct implications for die design and lubrication strategies. In addition, Liu et al. [27] employed HyperXtrude with an ALE formulation to simulate porthole die extrusion of a high length–width ratio aluminum profile and identified die design modifications that greatly improved flow uniformity and die performance, with results confirmed by experiment.

However, these commercial tools currently do not include dedicated physical models for nitrogen cooling, particularly in the presence of two-phase flow and transient operating conditions. As a result, advanced nitrogen cooling models are typically implemented in multiphysics environments that currently do not capture all relevant aspects of the extrusion process at the same level of the dedicated software, while commercial extrusion software accurately describes process mechanics but lacks a physically consistent representation of nitrogen cooling phenomena.

Within this framework, the present work aims to bridge the gap between advanced nitrogen cooling models and industrial extrusion simulation tools by proposing a dual-step procedure for the transient numerical analysis of multiple billets with nitrogen cooling. In the first step, a one-dimensional numerical model of nitrogen cooling is solved in a simplified environment using COMSOL Multiphysics, reproducing extrusion thermal conditions with negligible computational cost. The resulting heat transfer coefficient and nitrogen temperature are then transferred to the extrusion process model and implemented in the QForm code as additional boundary conditions, which are not assumed to be constant along the cooling path but instead arise from the thermo-fluid-dynamic behavior imposed by the channel design, cooling parameters, and process conditions. This approach enables the fully three-dimensional extrusion simulation to account for nitrogen cooling effects not only on the thermal field but also on aluminum flow and die resistance, thereby exploiting the strengths of commercial extrusion software while incorporating a physical description of nitrogen cooling phenomena.

2 Experimental Setting of the Selected Case Study

The experimental case study addressed several aspects of the extrusion process, including material flow, extrusion defects, welding quality, microstructure evolution, and the effects of nitrogen cooling, and was extensively detailed in [5]. Therefore, in the present paper, only the main aspects related to the analysis of the thermal field within the tooling set, under both uncooled and cooled conditions, are summarized and discussed. The study focused on the extrusion of fifteen AA6082 billets (279 mm diameter, 680 mm length) at a constant ram speed of 4.4 mm/s through a three-port porthole die, as illustrated in Fig. 1a, while Fig. 1b shows the geometry of the nitrogen cooling channel machined on the backer surface in contact with the die. Nitrogen cooling was applied from the sixth to the twelfth billet in order to investigate its influence on the thermal evolution of the tooling.

The die assembly—manufactured in AISI H13 steel and pre-heated to 480 °C—was instrumented with eleven K-type thermocouples strategically positioned to capture both global and highly localized thermal gradients as shown in Fig. 2. Six thermocouples (T1–T6) were embedded along the die surface in direct contact with the nitrogen-cooling channel, enabling a detailed reconstruction of the thermal evolution induced by nitrogen flow along the entire cooling path. Three additional sensors (T7–T9) were placed near the bearing exits of the three profiles to monitor tool temperatures in regions most directly affected by deformation heating and metal flow. A thermocouple positioned in the mandrel (T10) recorded the internal temperature of the tooling set near the feeding zone, while

T11, located in the vicinity of the die ring, provided information on the coldest structural component. In addition, a contactless pyrometer was used to monitor the temperature of profile 1 at a distance of 1500 mm from the die exit, allowing the thermal state of the extrudate to be assessed.

In section 3.2 Fig. 4 provide a schematic representation of the cooling-channel layout, highlighting the variations in channel cross-section along the cooling path. Starting from the central junction, the channel branches surrounding the three exiting profiles exhibit different cross-sectional areas, which were introduced with the aim of balancing the nitrogen mass flow. Profile 3 is more directly supplied by the main branch and is therefore more easily reached by the nitrogen flow. The process parameters adopted both in the experimental campaign and in the numerical model are summarized in Table 1 (see Section 3.2).

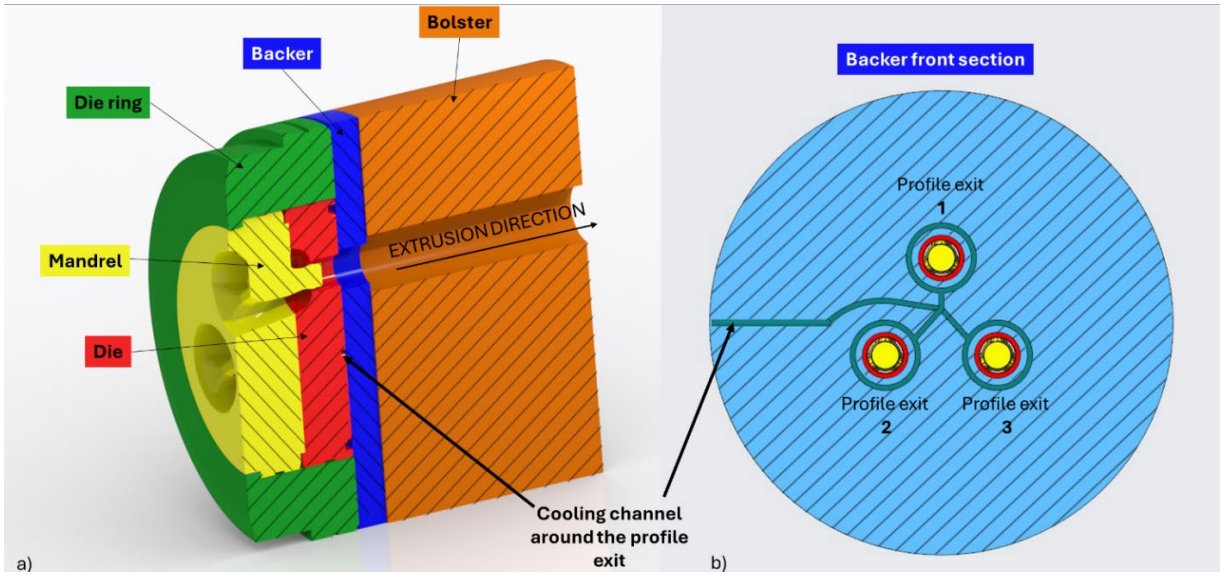

Fig. 1 a) Extrusion die assembly; b) Backer front view with cooling channel design.

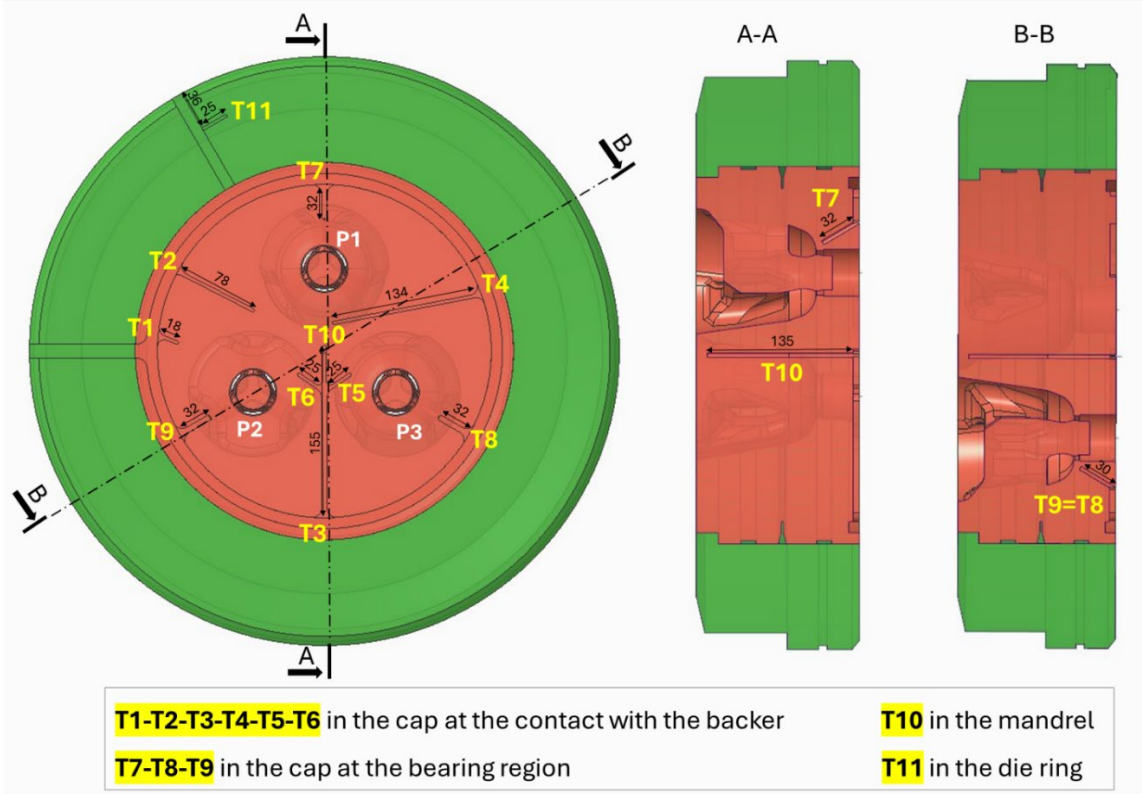

Fig. 2 Front view and sections of the die with thermocouple positions.

3.1 1D Numerical Model of nitrogen cooling

The accuracy and limitations of the 1D model combined with the Homogeneous Flow Model (HFM) approach have been demonstrated and discussed in previous works by Pelaccia and Santangelo [19,21]. In the present study, this framework is employed within a dual-step modeling strategy, where a dedicated 1D simulation of the cooling channel is performed to evaluate effective heat transfer coefficients (HTCs) reproducing the thermal effect of nitrogen cooling, which are subsequently imposed in the full extrusion model. The continuity and momentum conservation equations for nitrogen flow are solved along the streamwise direction of the cooling channel, assuming fully developed flow over its entire length:

$$\frac{\partial A_c \rho}{\partial t} + \nabla \cdot (A_c \rho u) = 0 \tag{1}$$

$$\rho \left[\frac{\partial u}{\partial t} + (u \cdot \nabla) u \right] = -\nabla p - \frac{1}{2} f_D \frac{\rho}{d_h} u|u| + F \tag{2}$$

where A_c is the channel cross-sectional area, ρ the fluid density, u the cross-section averaged velocity, p the pressure, t the time, f_D the Darcy friction factor, $d_h = 4A_c/P$ the hydraulic diameter, and F the gravitational body force. Local variations in channel geometry directly affect the hydraulic diameter, Reynolds number ($Re = \rho u d_h/\mu$), and pressure losses. The friction factor is evaluated using the Churchill correlation, valid for laminar, transitional, and turbulent regimes:

$$f_D = 8 \cdot \left\{ \left[\left(\frac{8}{Re} \right)^{12} (\theta_1 + \theta_2)^{-1.5} \right]^{\frac{1}{12}} \right\} \tag{3}$$

The energy equation is solved to predict the nitrogen temperature evolution along the cooling channel and the associated heat exchanged with the surrounding die:

$$\rho A_c c_p \frac{\partial T}{\partial t} + \rho A_c c_p u \cdot \nabla T = \nabla \cdot A_c k \nabla T + f_D \frac{\rho A_c}{2 d_h} u^3 + Q_{wall} \tag{4}$$

$$Q_{wall} = hP(T_{die} - T) \tag{5}$$

where c_p is the specific heat capacity at constant pressure, k the thermal conductivity, and Q_{wall} the heat exchanged per unit channel length with the die. In the dual-step approach, Q_{wall} is used exclusively to determine the equivalent convective heat transfer coefficient applied in the extrusion model. The term T_{die} is obtained, for each branch, from the simulation of the uncooled extrusion process performed within the QForm environment, in order to impose realistic thermal boundary conditions for the nitrogen cooling. In Eq. 5 h is the effective HTC and P the wetted perimeter. The HTC is obtained through the Nusselt number $Nu = hd_h/k$, assuming $Nu = 3.66$ for laminar flow and using the standard turbulent correlation:

$$Nu = \frac{\left(\frac{f_D}{8} \right) (Re - 1000) \cdot Pr}{1 + 12.7 \sqrt{\frac{f_D}{8}} \cdot \left(Pr^{\frac{2}{3}} - 1 \right)} \tag{6}$$

The two-phase conditions are considered through the HFM approach, where liquid and vapor phases are assumed to share the same velocity and no phase separation is considered, with the mixture properties expressed as functions of the liquid and gas mass fractions. In detail, density is defined as:

$$\rho = \left(\frac{\omega_g}{\rho_g} + \frac{\omega_l}{\rho_l}\right)^{-1} \tag{7}$$

while the dynamic viscosity follows the Einstein–Bedeaux formulation [19]:

$$\mu = \mu_l \cdot \phi_l^{-\left(\frac{\mu_l + 2.5\mu_g}{\mu_l + \mu_g}\right)} \tag{8}$$

with $\phi_l = (\rho/\rho_l)\omega_l$. Heat capacity and thermal conductivity of the mixture are computed using the model by Wang and Beckermann [19]:

$$\rho \cdot c_p = \omega_l \rho_l c_l + \omega_g \rho_g c_{p,g} \tag{9}$$

$$k = \omega_l k_l + \omega_g k_g \tag{10}$$

This formulation captures the relevant two-phase flow effects without explicitly resolving phase-change phenomena, since increasing gas mass fraction raises friction losses and reduces the Reynolds and Nusselt numbers, ultimately decreasing the convective heat transfer between nitrogen and the die walls. Thermophysical properties of liquid and gaseous nitrogen are assumed constant and evaluated at the atmospheric boiling point (−196 °C), since variations within the investigated pressure and temperature range remain below 10% [19]. The gas mass fraction is assumed to increase linearly with temperature [19], while pressure effects are neglected due to the limited pressure drop along the channel.

3.2 Implementation of the numerical dual step approach

The 3D-dimensional numerical simulation of the extrusion process was performed using QForm UK software 11.2.0.12, Fig. 3a, adopting the Eulerian module optimized for extrusion processes. The software includes an implemented capability to model cooling channel geometries within the die during geometric model preparation in the QShape module. The cooling channel geometry is imported as a separate solid model from the die CAD and, during mesh generation, the code automatically converts the solid into a channel machined within the die, as shown in Fig. 3b. The main simulation parameters are summarized in Table 1. The problem type ‘whole billet length simulation’ was selected to enable continuous simulation of the entire experimental extrusion campaign involving fifteen billets [5]. This approach allows the extrusion of multiple billets in sequence by assigning distinct temperature, speed, length, and stroke parameters to each billet.

To reproduce the pause times occurring experimentally during the loading of successive billets into the press, a virtual billet was introduced between two consecutive billets. This billet was extruded at an extremely low ram speed, resulting in a negligible contribution to the extrusion load, and with a very short length calculated to ensure that the duration of this dummy simulation matched the actual pause time of the experimental process. This approach enabled reproducing the entire experimental extrusion process, including the temperature variations occurring in the die during the pause periods, and extracting continuous time-dependent temperature and extrusion load data suitable for direct comparison with experimental measurements.

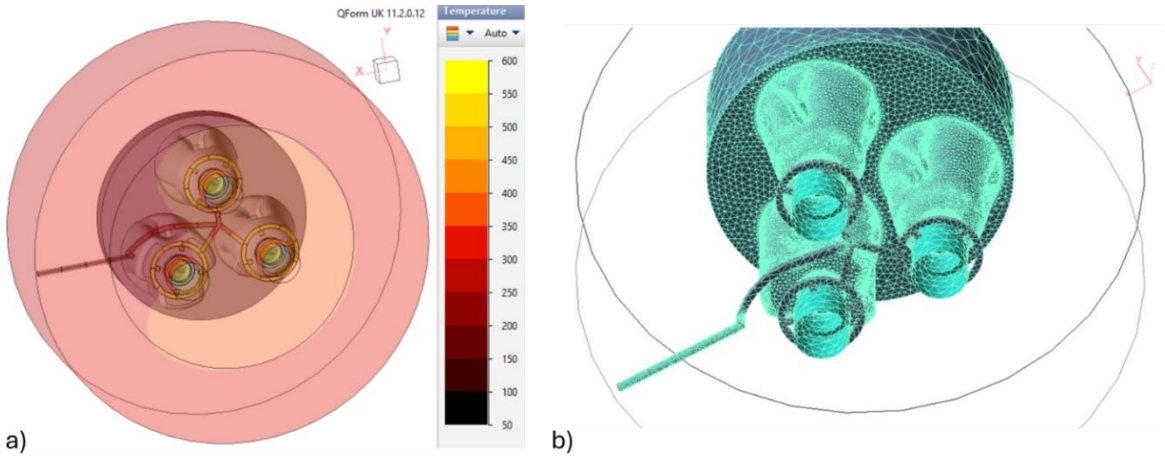

Fig. 3 a) Extrusion numerical simulation using Qform UK 11.2.0.12. b) Tooling set with cooling channel mesh generation within Qshape tool.

The extrusion process simulation under uncooled conditions was first carefully calibrated against experimental data to accurately reproduce the steady-state thermal field preceding the activation of liquid nitrogen cooling. In particular, the convective heat transfer coefficients applied to the external surfaces of the die ring and backer were calibrated to account for heat exchange with press components not explicitly included in the numerical model. Table 2 reports the temperature values of the die's component and the additional boundary conditions used to calibrate the uncooled 3D extrusion model. This preliminary calibration step was essential to ensure a reliable thermal reference condition for the subsequent cooled simulations.

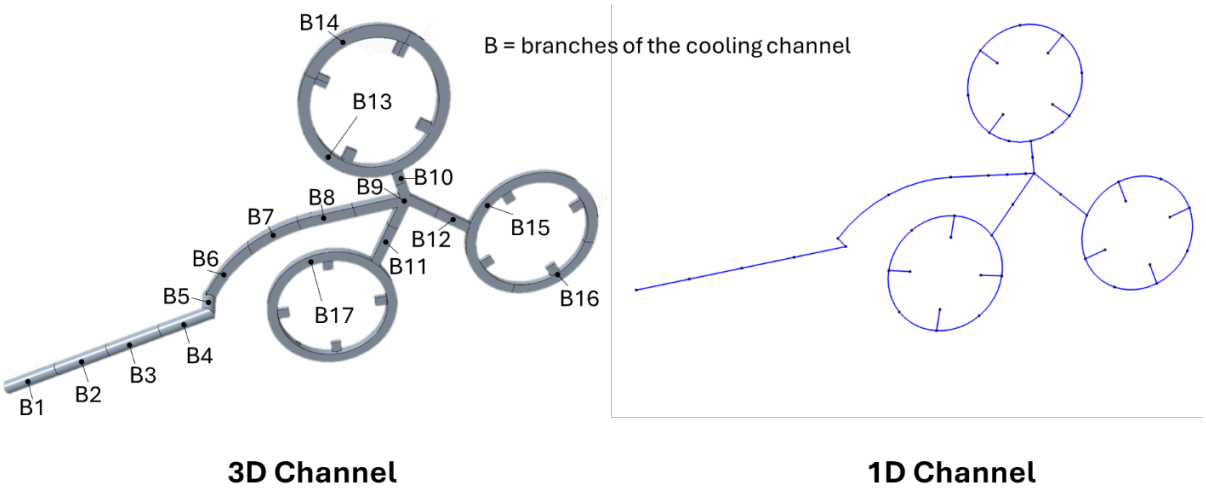

Fig. 4 3D and 1D representations of the cooling channel, segmented to apply varying temperature and heat transfer coefficient (HTC) boundary conditions.

Fig. 4 schematically illustrates the boundary-condition implementation adopted within the dual-step procedure. The cooling path was discretized into the same number of segments in both the three-dimensional extrusion model and the one-dimensional nitrogen-cooling model. Based on the results of the uncooled extrusion simulations, the average temperature of each segment of the cooling path was extracted and imposed as the boundary condition T_{die} (see section 3.1) for the corresponding channel segment in the 1D model. Conversely, starting from the sixth extrusion—corresponding to the first run with active liquid nitrogen cooling—convective thermal boundary conditions were applied to the channel surfaces in the 3D model, using the local heat transfer coefficients and nitrogen temperatures obtained from the 1D simulations. It is worth noting that, in this framework, the heat transfer coefficient is not uniform along the cooling path but progressively decreases as the gas mass fraction increases. Table 3 summarizes the boundary conditions adopted in both the 1D and 3D models. As can be observed, in regions located far from the nitrogen inlet, unfavorable thermal

exchange conditions may arise due to gas formation within the channel. For instance, sectors B14 and B16 recorded nitrogen temperatures exceeding 0 °C, indicating that heat transfer in these areas is significantly less effective than in upstream regions.

Finally, the material properties of the AA6082 alloy billets were defined by the main parameters summarized in Table 4. The alloy flow stress was characterized by hot torsion testing and implemented in the software using a five-parameter Hensel–Spittel constitutive model, with coefficients listed in Table 5 [5, 28].

Table 1 Extrusion process parameters.

Process Parameter	Value
Profile alloy	AA6082
Billet diameter	279 [mm]
Container diameter	286 [mm]
Billet length	680 [mm]
Billet rest	30 [mm]
Ram speed	4.4 [mm/s]
Max press load	40 [MN]
Pre-heating Billet temperature	480 [°C]

Table 2 Temperature and HTC values applied to die-set components and boundary conditions.

Object/Boundary	Temperature [°C]	HTC [W/(m^{2}K)]
Die set	480	-
Bolster	350	-
Ram (Dummy block)	370	-
Container	435 close to die set-400 end	-
Environment (Air)	20	30
Die Holder	270	3000
Pressure ring	350	3000

Table 3 Boundary conditions applied to the different branches defined along the cooling channel path.

N° branch of cooling channel	Cross- section dimension [mm]	Temperature from Qform before cooling [°C]	HTC from Comsol [W/(m^{2}K)]	Temperature of Nitrogen from Comsol [°C]
B1	Ø 8	330	2776.6	-195.5
B2	Ø 8	355	2232.4	-194.7
B3	Ø 8	370	1763	-193.9
B4	Ø 8	378	1369.8	-193.2
B5	Ø 8	390	1115.5	-192.6
B6	6 x 6	400	1310.4	-192
B7	6 x 6	410	1277.9	-191
B8	6 x 6	410	1277.9	-191
B9	6 x 6	410	1277.9	-189.4
B10	6 x 5	410	279.27	-189
B11	6 x 5	410	193.7	-188.7
B12	6 x 3.5	410	50	-189
B13	6 x 5	410	34.5	-188.5
B14	6 x 5	410	34	7
B15	6 x 3.5	410	50	-188
B16	6 x 3.5	410	34.5	150
B17	6 x 5	410	34.5	-188.5

Table 4 AA6082 material properties.

Material Properties	AA6082
Density	2608 [kg/m^3]
Specific heat	1017 [J/(kg·K)]
Thermal conductivity	217 [W/(m·K)]
Thermal expansion	2.73e-5 [1/°C]
Young's modulus	69000 [MPa]
Poisson's ratio	0.33

Table 5 AA6082 Flow stress coefficient with temperature expressed in °C.

Hensel-Spittel model	Parameters
A	98.851 [MPa]
m1	-0.0022408
m2	-0.0405691
m3	0.105639
m4	-0.0012775
m5	0
m7	0
m8	0
m9	0

4 Experimental-Numerical Assessment of Thermal Fields during Multiple Extrusion Runs: Results and Discussion

Fig. 5 and Fig. 6 present the experimental–numerical comparisons of the thermal evolution recorded by the thermocouples over the entire extrusion campaign, from the positioning of the tooling set inside the press to the extrusion of the fifteenth billets. For clarity of presentation, the results were grouped according to the temperature ranges reached at the different measurement locations. Accordingly, Fig. 5 reports the comparison for thermocouples T7–T10 together with the pyrometer signal, while Fig. 6 focuses on thermocouples T1–T6 and T11.

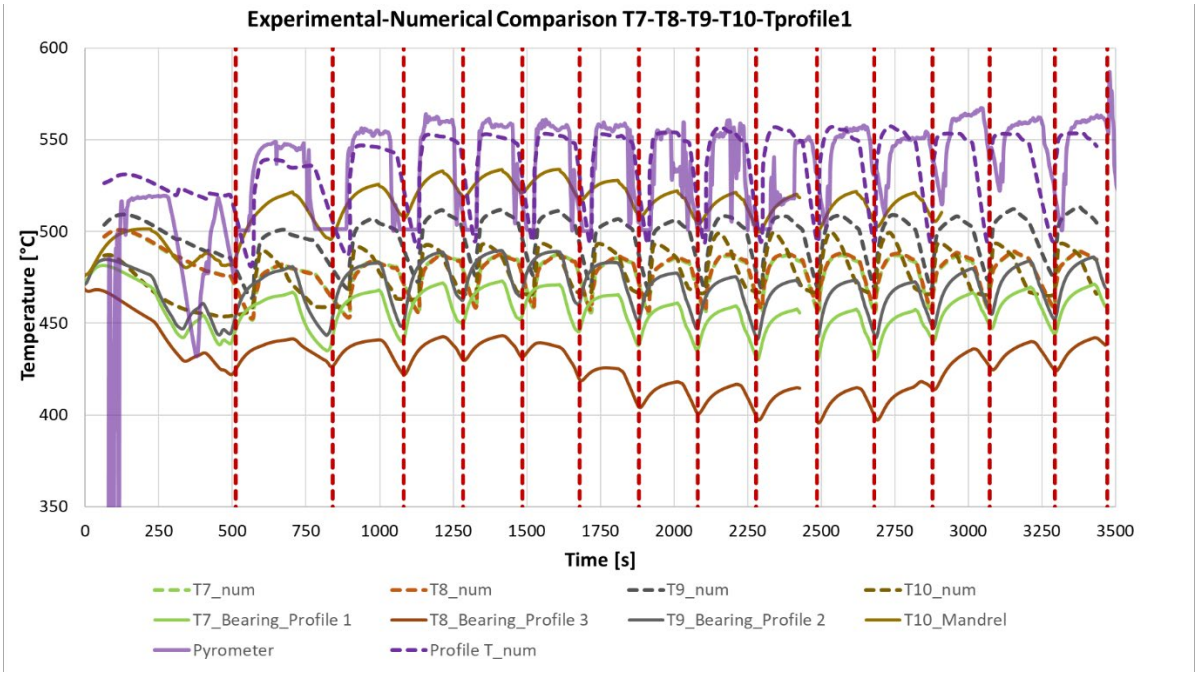

Fig. 5 Experimental-numerical comparison of temperatures T7–T10 and the profile's temperature.

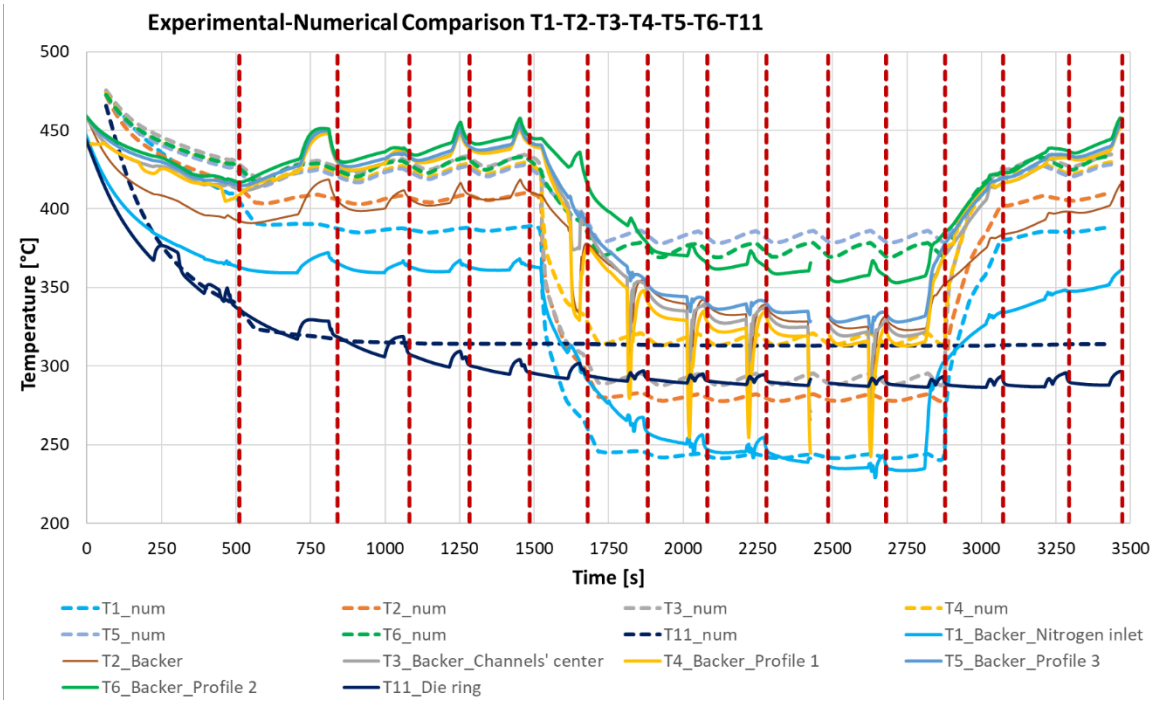

Fig. 6 Experimental-numerical comparison of temperatures T1–T11.

From experimental data, it can be observed that before extrusion the die underwent a significant temperature decrease during loading into the press, with values dropping from the oven temperature of 480 °C to between 445 and 476 °C, depending on the measurement location. During the first extrusion the thermal field evolved under the combined influence of frictional and deformation heating, together with conductive and radiative heat losses to the press. At the beginning of the second extrusion, deformation heating became dominant, resulting in a marked temperature stratification within the tooling set. Temperatures measured near the bearings ranged between approximately 441 °C during billet change and 480 °C during extrusion, while the mandrel (T10) reached the highest value, peaking at about 520 °C. In contrast, the die ring (T11) remained significantly cooler, around 330 °C, highlighting the pronounced heat-sink effect of the surrounding press components. Starting from the fourth run, a quasi steady-state thermal condition was reached, as indicated by negligible temperature differences with the fifth run. Under these uncooled steady-state conditions, temperatures stabilized at approximately 430–445 °C in the backer region, 468–490 °C near the bearings, and around 530 °C in the mandrel, while the pyrometer recorded an exit temperature of roughly 560 °C for profile 1. It should be noted that the temperatures measured near the bearings are relatively low when compared with those recorded in the mandrel. This indicates that the locations of thermocouples T7–T9 are not sufficiently close to the bearings to capture the actual thermal gradients in the regions where the highest temperatures are expected.

The numerical model, including appropriate boundary conditions and the introduction of virtual extrusions associated with billet changes, is able to accurately reproduce both the initial thermal transient and the attainment of steady-state conditions. More specifically, in the backer region (T1–T6), an almost perfect numerical–experimental agreement is achieved for all thermocouples, with the exception of T1, where the numerical model slightly overestimates the temperature by a maximum of approximately 25 °C, while still correctly reproducing the overall thermal trend. Since the temperature measured at T11, positioned close to the external surface of the die ring, is accurately predicted, this discrepancy is more likely attributable to a displacement of the thermocouple from its nominal position rather than to an incorrect thermal exchange between the die and the die ring.

Focusing on the die–mandrel region (T7–T10), good agreement is obtained for T7 and T9, with discrepancies below 20 °C, whereas a larger overestimation of about 40 °C is observed at T8 (480 °C vs 440 °C). However, the experimental value appears unusually low for a location close to the bearings, especially when compared with the temperatures measured at the other two exits (between 470 °C and 490 °C). In the numerical model, the bearing temperatures at the three exits are indeed

predicted to be very similar, suggesting with high confidence that thermocouple T8 was displaced within its housing. In the mandrel, at the position of T10, a maximum numerical underestimation of approximately 30 °C is observed (500 °C versus 530 °C). This discrepancy is reduced when considering the profile exit temperature, where the numerical underestimation decreases to about 15 °C (545 °C versus 560 °C). Also in this case, given the agreement obtained for the extrudate temperature, a possible forward displacement of thermocouple T10 along the extrusion direction cannot be excluded, where temperature rises rapidly as the welding chamber is approached. At the nominal T10 position, a lower temperature could be expected due to its proximity to the feeding zone, which is influenced by the incoming billet temperature (approximately 480 °C). It cannot be excluded that the high thermal gradient measured by thermocouple T10 is representative of the actual thermal field in the mandrel region; consequently, the observed numerical discrepancy may be attributed to other modeling aspects, such as the imposed flow stress of the deforming material, which directly influences the amount of deformation heating generated [28-29]. Despite these aspects, the calibration of the uncooled numerical model can be considered highly satisfactory, especially given the complexity of reproducing the initial thermal transient and the continuous extrusion process over multiple billets with intermediate billet changes.

Nitrogen cooling was activated at the beginning of the sixth extrusion by fully opening the supply valve (liquid nitrogen at −196 °C and 3 bar). During the first nitrogen-cooled runs, T1 (located near the inlet channel) temperature rapidly decreased from approximately 365 °C to 265 °C within two billets and eventually stabilized at about 234 °C by the twelfth extrusion. However, the response of the remaining thermocouples revealed a non-uniform and asymmetric cooling distribution along the channel. For example, T6—located near profile 2—reached a steady-state temperature of about 360 °C, remaining roughly 40 °C higher than T3 and T4, positioned in the central portion of the channel and stabilizing around 320 °C. Measurements near the bearing exits further confirmed this unbalanced cooling behavior. The most pronounced temperature reduction occurred at T8 (exit 3), where temperatures decreased from approximately 445 °C to 417 °C, whereas T7 (exit 1) and T9 (exit 2) exhibited only limited reductions of about 10 °C. The cooling effect did not significantly extend to the mandrel, whose temperature remained nearly unchanged at approximately 520 °C, indicating that the cooling channel was too distant from this region to exert a meaningful thermal influence. Consistently, the pyrometer recorded only a modest reduction of about 10 °C in the profile exit temperature (from 560 °C to 550 °C), confirming that the overall cooling effectiveness was constrained by the poorly designed cooling channel layout rather than by the intrinsic cooling capability of liquid nitrogen.

When nitrogen flow was switched off during the final three extrusions, temperatures at all thermocouple locations progressively increased toward the initial uncooled steady-state values, further confirming the reproducibility of the thermal-field measurements and the direct correlation between the observed temperature variations and nitrogen cooling.

From the numerical results, an excellent experimental–numerical agreement is also achieved under cooled conditions. The thermal field along the entire cooling path is predicted with very good accuracy, with an almost perfect overlap of temperature evolutions for all backer thermocouples, except for T5, where the cooling effect is underestimated by approximately 35 °C. This discrepancy suggests that, within the 1D nitrogen-cooling model, the HFM approach slightly underestimates the local heat-transfer effectiveness in the region surrounding thermocouple T5. Nevertheless, considering the simplified and computationally efficient approach adopted to derive the HTC reproducing the nitrogen-cooling effect, the quality of the results can be regarded as overall satisfactory. The numerical model also correctly predicts the negligible influence of nitrogen cooling on the mandrel and die, further confirming its reliability in reproducing the thermal field and, consequently, in assessing the effectiveness of the designed cooling system. In addition, the model accurately captures the temperature increase during the final cycles in which the cooling system was switched off.

Finally, Fig. 7 reports the numerical–experimental comparison of the extrusion force. The solid green curve represents the force measured during the extrusion of all 15 billets, whereas the dashed green curve corresponds to the extrusion force predicted by the numerical simulation. It can be clearly observed that, after the first billet characterized by transient conditions, an excellent overlap between experimental and numerical data is achieved starting from the second billet onward. This agreement demonstrates that the numerical simulation is able to accurately predict the extrusion load throughout the steady-state extrusion cycles.

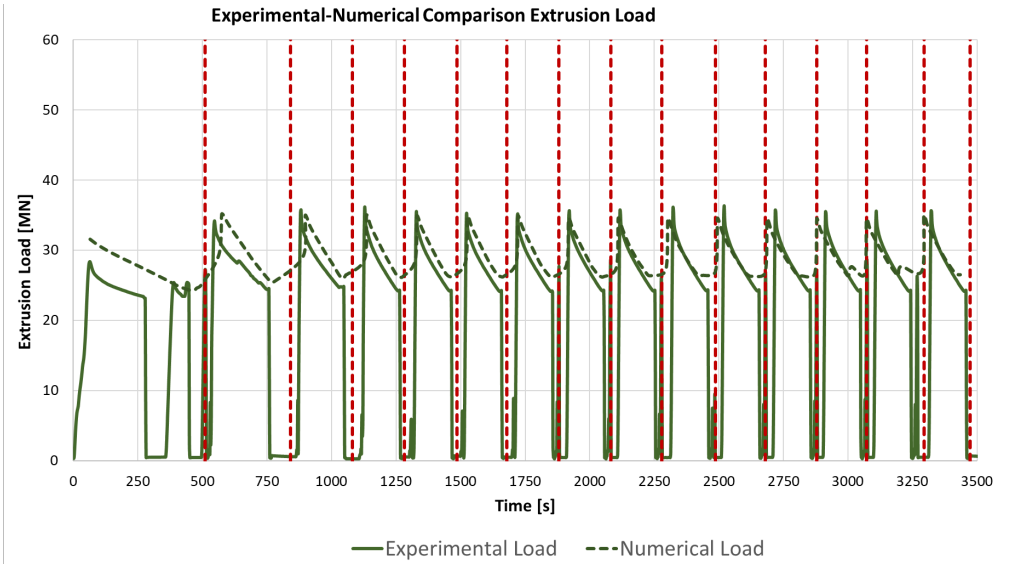

Fig. 7 Experimental-numerical comparison of extrusion load.

Overall, the results demonstrate the capability of the proposed dual-step procedure to integrate nitrogen-cooling effects into commercial extrusion software through a simplified and reliable approach. Although the cooling system, designed primarily on empirical experience, did not significantly reduce bearing temperatures in this study, the model provides the capability to assess thermal gradients and their potential influence on flow stress, velocity distribution at the profile exit, and die stress.

5 Summary

A dual-step numerical framework was developed by coupling a one-dimensional homogeneous-flow model of the nitrogen cooling channel with a three-dimensional extrusion simulation in QForm. The methodology was validated against an industrial campaign of fifteen AA6082 billets instrumented with eleven thermocouples. Under uncooled steady-state conditions, temperatures stabilized at 430–445 °C in the backer, 468–490 °C near the bearings, about 530 °C in the mandrel, and 560 °C at the profile exit. Numerical predictions generally differed by less than 20 °C, with a maximum deviation of about 30 °C, which can be considered highly satisfactory given the complexity of reproducing the initial thermal transient and the continuous extrusion of multiple billets. The extrusion force was accurately reproduced from the second billet onward, showing excellent agreement during steady-state operation.

When liquid nitrogen cooling was activated, the temperature near the channel inlet decreased from 365 °C to 234 °C, while downstream locations stabilized between 320 °C and 360 °C. The maximum reduction at the bearing exits was about 28 °C, and the profile exit temperature decreased by approximately 10 °C. The model reproduced both the magnitude and spatial distribution of these variations, as well as the temperature recovery after cooling deactivation.

These results demonstrated that the proposed dual-step procedure is able to reproduce the transient thermal evolution over multiple billets, exploiting the computational efficiency of a 1D cooling model coupled with an industrial 3D extrusion simulation environment. Overall, this approach enables the simultaneous evaluation of thermal gradients induced by the cooling channels and their interaction

with key technological aspects of the extrusion process, including aluminum flow, deformation heating, extrusion load, and die thermal response. In this way, the strengths of advanced cooling models are combined with the comprehensive process description provided by commercial extrusion software.

Acknowledgements

This work was supported by PNRR–M4C2INV1.5, NextGenerationEU-Avviso 3277/2021 - ECS_00000033 ECOSISTER-spk 3

References

[1] T. Sheppard, Extrusion of Aluminium Alloys, Springer, London, 1999.

[2] D. Leśniak, J. Zasadziński, W. Libura, Z. Gronostajski, R. Śliwa, B. Leszczyńska-Madej, M. Kaszuba, A. Woźnicki, B. Płonka, P. Widomski & J. Madura, Latest Advances in Extrusion Processes of Light Metals, Archives of Civil and Mechanical Engineering, 24 (2024) 184.

[3] D. Pietzka, N. Ben Khalifa, L. Donati, L. Tomesani, A.E. Tekkaya, Extrusion Benchmark 2009: Experimental analysis of deflection in extrusion dies, Key Engineering Materials 424 (2009) 19–26.

[4] L. Donati, A. Segatori, A. Gamberoni, B. Reggiani, L. Tomesani, Extrusion Benchmark 2017: Effect of Die Design on Profile Quality and Distortions of Thin C-Shaped Hollow Profiles, Materials Today: Proceedings, 10:2 (2019) 171-184.

[5] R. Pelaccia, M. Negozio, S. Di Donato, B. Reggiani, L. Donati, Extrusion Benchmark 2023: Effect of die design on profile speed, seam weld quality and microstructure of hollow tubes, Key Engineering Materials 988 (2024) 47–62

[6] L. Donati, B. Reggiani, R. Pelaccia et al., Advancements in extrusion and drawing: a review of the contributions by the ESAFORM community, International Journal of Material Forming 15 (2022) 41.

[7] M. Özcan, C. Ozsut, O. Deveci, G. Bentesen, The effect of nitrogen gas cooling used in aluminium extrusion molds on production efficiency, Open Journal of Applied Sciences 10 (2021) 414–421.

[8] D.H. Ko, B.H. Kang, D.C. Ko et al., Improvement of mechanical properties of Al6061 extrudate by die cooling with N_2 gas during hot extrusion, Journal of Mechanical Science and Technology 27 (2013) 153–161.

[9] L. Donati, A. Segatori, B. Reggiani, L. Tomesani, P.A. Bevilacqua Fazzini, Effect of liquid nitrogen die cooling on extrusion process conditions, Key Engineering Materials 491 (2012) 215–222.

[10] A.F. Ciuffini, S. Barella, C. Di Cecca, A. Gruttadauria, C. Mapelli, L. Merello, G. Mainetti, M. Bertoletti, Surface Quality Improvement of AA6060 Aluminum Extruded Components through Liquid Nitrogen Mold Cooling, Metals 8 (2018) 409.

[11] E. Giarmas, D. Tzetzis, Effect of increased extrusion ram speed and liquid nitrogen cooling on the mechanical properties of 6060 aluminum alloy, Metals 15 (2025) 1136.

[12] E. Giarmas, E. Tzimtzimis, D. Tzetzis, The influence of ageing conditions and liquid nitrogen cooling of extrusion dies on nanoindentation creep in 6060 aluminium alloy, International Journal of Advanced Manufacturing Technology 137 (2025) 6187–6205.

[13] R. Pelaccia, B. Reggiani, M. Negozio, L. Donati, Liquid nitrogen in the industrial practice of hot aluminium extrusion: experimental and numerical investigation, International Journal of Advanced Manufacturing Technology 119 (2022) 3141–3155.

[14] R. Hölker, A. Jäger, N. Ben Khalifa, A.E. Tekkaya, New concepts for cooling of extrusion dies manufactured by rapid tooling, Key Engineering Materials 491 (2011) 223–232.

[15] R. Pelaccia, M. Negozio, L. Donati, L.Tomesani, Extrusion of light and ultralight alloys with liquid nitrogen conformal cooled dies: process analysis and simulation, Journal of Materials Engineering and Performance 31 (2022) 1991–2001

[16] A. Armillotta, R. Baraggi, S. Fasoli, SLM tooling for die casting with conformal cooling channels, International Journal of Advanced Manufacturing Technology 71 (2014) 573–583.

[17] B.B. Kanbur, S. Suping, F. Duan, Design and optimization of conformal cooling channels for injection molding: a review, International Journal of Advanced Manufacturing Technology 106 (2020) 3253–3271.

[18] E. Giarmas, V. Tsakalos, E. Tzimtzimis, N. Kladovasilakis, I. Kostavelis, D. Tzovaras, D. Tzetzis, Selective laser melting additive manufactured H13 tool steel for aluminum extrusion die component construction, International Journal of Advanced Manufacturing Technology 133 (2024) 4385–4400.

[19] R. Pelaccia, M. Negozio, S. Di Donato, L. Donati, B. Reggiani, Recent trends in nitrogen cooling modelling of extrusion dies, Key Engineering Materials 987 (2024) 11–22.

[20] A. Husain, Applicability of the Homogeneous Flow Model to Two-Phase Flow, PhD Thesis, University of Cincinnati, 1975.

[21] R. Pelaccia, P.E. Santangelo, A homogeneous-flow model for nitrogen cooling in the aluminum-alloy extrusion process, International Journal of Heat and Mass Transfer 195 (2022) 123-202.

[22] R. Pelaccia, M. Negozio, B. Reggiani, L. Donati, Assessment of the optimization strategy for nitrogen cooling channel design in extrusion dies, Key Engineering Materials 926 (2022) 460–470.

[23] A. Biba, S. Stebunov, A. Lishny, Simulation of material flow coupled with die analysis in complex shape extrusion, Key Engineering Materials (2013)..

[24] I. Kniazkin, N. Biba, I. Kulakov, A. Duzhev, S. Stebunov, Die Design, Extrusion, Optimisation, SimulationAutomated Optimum Extrusion Die Design and Profile Quality Control Based on Simulation, Key Engineering Materials 505 (2024) 85-92.

[25] S. Koloskov, S. Sidelnikov, D. Voroshilov, Modeling Process of Semi-Continuous Extrusion of Hollow 6063 Aluminum Alloy Profiles Using QForm Extrusion, Solid State Phenomena 316 (2021) 288-294.

[26] S. E. Hoque, S. Hovden, S. Culic, J. A. Nietsch, J. Kronsteiner, D. Horwatitsch, Modeling Friction in HyperXtrude for Hot Forward Extrusion Simulation of EN AW 6060 and EN AW 6082 Alloys, Key Engineering Materials 926 (2022) 416-425.

[27] Z. Liu, L. Li, S. Li, J. Yi, G. Wang, Simulation analysis of porthole die extrusion process and die structure modifications for an aluminum profile with high length–width ratio and small cavity, Materials 11 (2018) 1517.

[28] S. Di Donato, R. Pelaccia, M. Negozio, M.E. El Mehtedi, B. Reggiani, L. Donati, Hot torsion tests of AA6082 alloy, Key Engineering Materials 988 (2024) 21–29.

[29] S. Di Donato, R. Pelaccia, M. Negozio, N. Lai, M. El Mehtedi, B. Reggiani, L. Donati, Effect of material characterization via torsion tests on the accuracy of FEM simulations in the extrusion process, Materials Research Proceedings 54 (2025) 780-791.